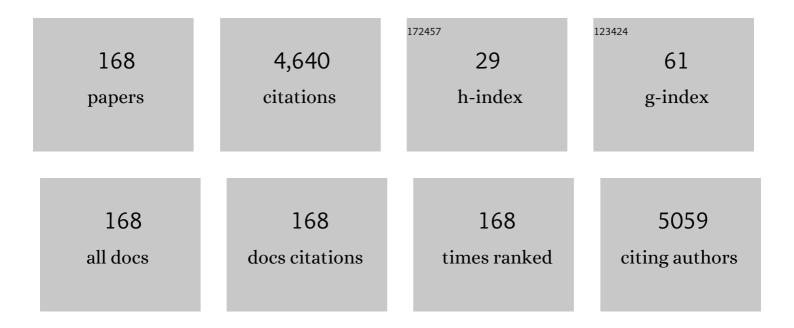
## Sung-Jin Choi

List of Publications by Year in descending order

Source: https://exaly.com/author-pdf/7803851/publications.pdf Version: 2024-02-01



SUNC-IN CHOI

#	Article	IF	CITATIONS
1	Total Subgap Range Density of States-Based Analysis of the Effect of Oxygen Flow Rate on the Bias Stress Instabilities in a-IGZO TFTs. IEEE Transactions on Electron Devices, 2022, 69, 166-173.	3.0	15
2	Cost-effective method for fabricating carbon nanotube network transistors by reusing a 99% semiconducting carbon nanotube solution. Nanotechnology, 2022, 33, 24LT01.	2.6	0
3	All-Solution-Processed Carbon Nanotube Floating Gate Memories. ACS Applied Nano Materials, 2022, 5, 7652-7657.	5.0	1
4	Pâ€30: Thermally Activated and Fieldâ€Enhanced Diffusion of Dopants in aâ€InGaZnO TFTs Under Circuit Operations and Correlation to Device Stabilities. Digest of Technical Papers SID International Symposium, 2022, 53, 1149-1152.	0.3	0
5	Defect spectroscopy of sidewall interfaces in gate-all-around silicon nanosheet FET. Nanotechnology, 2021, 32, 165202.	2.6	3
6	Humidity Effects According to the Type of Carbon Nanotubes. IEEE Access, 2021, 9, 6810-6816.	4.2	9
7	Low-Power True Random Number Generator Based on Randomly Distributed Carbon Nanotube Networks. IEEE Access, 2021, 9, 91341-91346.	4.2	4
8	Analysis of Threshold Voltage Shift for Full VGS/VDS/Oxygen-Content Span under Positive Bias Stress in Bottom-Gate Amorphous InGaZnO Thin-Film Transistors. Micromachines, 2021, 12, 327.	2.9	11
9	Multiplexed Silicon Nanowire Tunnel FET-Based Biosensors With Optimized Multi-Sensing Currents. IEEE Sensors Journal, 2021, 21, 8839-8846.	4.7	12
10	Observation of Hydrogen-Related Defect in Subgap Density of States and Its Effects Under Positive Bias Stress in Amorphous InGaZnO TFT. IEEE Electron Device Letters, 2021, 42, 708-711.	3.9	14
11	Observation of Divacancy Formation for ZnON Thin-Film Transistors With Excessive N Content. IEEE Electron Device Letters, 2021, 42, 1006-1009.	3.9	1
12	Characterization of Spatial Distribution of Trap Across the Substrate in Metal-Insulator-Semiconductor Structure with Band Bending Effect. Journal of Nanoscience and Nanotechnology, 2021, 21, 4315-4319.	0.9	0
13	Current-to-transconductance ratio technique for simultaneous extraction of threshold voltage and parasitic resistances in MOSFETs. Solid-State Electronics, 2021, 183, 108133.	1.4	3
14	Modeling and characterization of photovoltaic and photoconductive effects in insulated-gate field effect transistors under optical excitation. Solid-State Electronics, 2021, 186, 108139.	1.4	1
15	Threshold-Variation-Tolerant Coupling-Gate α-IGZO Synaptic Transistor for More Reliably Controllable Hardware Neuromorphic System. IEEE Access, 2021, 9, 59345-59352.	4.2	10
16	Parallel weight update protocol for a carbon nanotube synaptic transistor array for accelerating neuromorphic computing. Nanoscale, 2020, 12, 2040-2046.	5.6	28
17	Positive Bias Stress Instability of InGaZnO TFTs With Self-Aligned Top-Gate Structure in the Threshold-Voltage Compensated Pixel. IEEE Electron Device Letters, 2020, 41, 50-53.	3.9	10
18	Density-of-States-Based Physical Model for Ink-Jet Printed Thiophene Polymeric TFTs. IEEE Transactions on Electron Devices, 2020, 67, 283-288.	3.0	1

Sung-Jin Choi

#	Article	IF	CITATIONS
19	Alternating Current-Based Technique for Separate Extraction of Parasitic Resistances in MISFETs With or Without the Body Contact. IEEE Electron Device Letters, 2020, 41, 1528-1531.	3.9	3
20	Understanding the signal amplification in dual-gate FET-based biosensors. Journal of Applied Physics, 2020, 128, .	2.5	17
21	16-Bit Fixed-Point Number Multiplication With CNT Transistor Dot-Product Engine. IEEE Access, 2020, 8, 133597-133604.	4.2	3
22	Effect of Anion Composition on the Bias Stress Stability in Zn-O-N Thin-Film Transistors. IEEE Electron Device Letters, 2020, 41, 1376-1379.	3.9	1
23	One Transistor–Two Memristor Based on Amorphous Indium–Gallium–Zinc-Oxide for Neuromorphic Synaptic Devices. ACS Applied Electronic Materials, 2020, 2, 2837-2844.	4.3	21
24	Pd/IGZO/p <sup>+</sup> -Si Synaptic Device with Self-Graded Oxygen Concentrations for Highly Linear Weight Adjustability and Improved Energy Efficiency. ACS Applied Electronic Materials, 2020, 2, 2390-2397.	4.3	17
25	Extraction Technique for Flat Band Voltage Using Multi-Frequency C – V Characteristics in Amorphous InGaZnO Thin-Film-Transistors. IEEE Electron Device Letters, 2020, 41, 1778-1781.	3.9	2
26	Digital and Analog Switching Characteristics of InGaZnO Memristor Depending on Top Electrode Material for Neuromorphic System. IEEE Access, 2020, 8, 192304-192311.	4.2	23
27	Deep depletion capacitance–voltage technique for spatial distribution of traps across the substrate in MOS structures. Solid-State Electronics, 2020, 173, 107905.	1.4	0
28	A tactile sensor system with sensory neurons and a perceptual synaptic network based on semivolatile carbon nanotube transistors. NPG Asia Materials, 2020, 12, .	7.9	12
29	Directly drawn top-gate semiconducting carbon nanotube thin-film transistors and complementary inverters. Nanotechnology, 2020, 31, 32LT01.	2.6	4
30	Experimental extraction of stern-layer capacitance in biosensor detection using silicon nanowire field-effect transistors. Current Applied Physics, 2020, 20, 828-833.	2.4	12
31	Hybrid integration of carbon nanotube and amorphous IGZO thin-film transistors. AIP Advances, 2020, 10, .	1.3	5
32	Influence of Nitrogen Content on Persistent Photoconductivity in Zinc Oxynitride Thin Film Transistors. IEEE Electron Device Letters, 2020, 41, 561-564.	3.9	4
33	Design study of the gate-all-around silicon nanosheet MOSFETs. Semiconductor Science and Technology, 2020, 35, 03LT01.	2.0	27
34	Wafer-scale carbon nanotube network transistors. Nanotechnology, 2020, 31, 465303.	2.6	6
35	Characterization of Subgap Density-of-States by Sub-Bandgap Optical Charge Pumping in In <sub>0.53</sub> Ga <sub>0.47</sub> As Metal-Oxide-Semiconductor Field-Effect Transistors. Journal of Nanoscience and Nanotechnology, 2020, 20, 4287-4291.	0.9	0
36	Influence of the Gate/Drain Voltage Configuration on the Current Stress Instability in Amorphous Indium-Zinc-Oxide Thin-Film Transistors With Self-Aligned Top-Gate Structure. IEEE Electron Device Letters, 2019, 40, 1431-1434.	3.9	7

#	Article	IF	CITATIONS
37	Flexible carbon nanotube Schottky diode and its integrated circuit applications. RSC Advances, 2019, 9, 22124-22128.	3.6	13
38	Ultrasensitive Electrical Detection of Hemagglutinin for Point-of-Care Detection of Influenza Virus Based on a CMP-NANA Probe and Top-Down Processed Silicon Nanowire Field-Effect Transistors. Sensors, 2019, 19, 4502.	3.8	24
39	Precision-extension technique for accurate vector–matrix multiplication with a CNT transistor crossbar array. Nanoscale, 2019, 11, 21449-21457.	5.6	10
40	Impact of Synaptic Device Variations on Classification Accuracy in a Binarized Neural Network. Scientific Reports, 2019, 9, 15237.	3.3	20
41	Effect of Oxygen Content on Current Stress-Induced Instability in Bottom-Gate Amorphous InGaZnO Thin-Film Transistors. Materials, 2019, 12, 3149.	2.9	44
42	Oxygen Content and Bias Influence on Amorphous InGaZnO TFT-Based Temperature Sensor Performance. IEEE Electron Device Letters, 2019, 40, 1666-1669.	3.9	6
43	Binarized Neural Network with Silicon Nanosheet Synaptic Transistors for Supervised Pattern Classification. Scientific Reports, 2019, 9, 11705.	3.3	9
44	Control of the Boundary between the Gradual and Abrupt Modulation of Resistance in the Schottky Barrier Tunneling-Modulated Amorphous Indium-Gallium-Zinc-Oxide Memristors for Neuromorphic Computing. Electronics (Switzerland), 2019, 8, 1087.	3.1	18
45	Effect of Simultaneous Mechanical and Electrical Stress on the Electrical Performance of Flexible In-Ga-Zn-O Thin-Film Transistors. Materials, 2019, 12, 3248.	2.9	17
46	The Influence of Anion Composition on Subgap Density of States and Electrical Characteristics in ZnON Thin-Film Transistors. IEEE Electron Device Letters, 2019, 40, 40-43.	3.9	8
47	Method to Extract Interface and Bulk Trap Separately Over the Full Sub-Gap Range in Amorphous InGaZnO Thin-Film Transistors by Using Various Channel Thicknesses. IEEE Electron Device Letters, 2019, 40, 574-577.	3.9	15
48	Synaptic behavior of flexible IGZO TFTs with Al <sub>2</sub> O <sub>3</sub> gate insulator by low temperature ALD. , 2019, , .		2
49	Carbon Nanotube Network Transistor for a Physical Unclonable Functions-based Security Device. , 2019, , .		2
50	SPICE compact model of IGZO memristor based on non-quasi statically updated Schottky barrier height. , 2019, , .		2
51	The Calculation of Negative Bias Illumination Stress-Induced Instability of Amorphous InGaZnO Thin-Film Transistors for Instability-Aware Design. IEEE Transactions on Electron Devices, 2018, 65, 1002-1008.	3.0	8
52	Three-Dimensionally Printed Micro-electromechanical Switches. ACS Applied Materials & Interfaces, 2018, 10, 15841-15846.	8.0	15
53	Impact of Synaptic Device Variations on Pattern Recognition Accuracy in a Hardware Neural Network. Scientific Reports, 2018, 8, 2638.	3.3	63
54	Impact of Ground Plane Doping and Bottom-Gate Biasing on Electrical Properties in In <sub>0.53</sub> Ga <sub>0.47</sub> As-OI MOSFETs and Donor Wafer Reusability Toward Monolithic 3-D Integration With In <sub>0.53</sub> Ga <sub>0.47</sub> As Channel. IEEE Transactions on Electron Devices, 2018, 65, 1862-1868.	3.0	14

#	Article	IF	CITATIONS
55	Effects of structure and oxygen flow rate on the photo-response of amorphous IGZO-based photodetector devices. Solid-State Electronics, 2018, 140, 115-121.	1.4	15
56	Effect of oxygen content of the LaAlO 3 layer on the synaptic behavior of Pt/LaAlO 3 /Nb-doped SrTiO 3 memristors for neuromorphic applications. Solid-State Electronics, 2018, 140, 139-143.	1.4	26
57	The electron trap parameter extraction-based investigation of the relationship between charge trapping and activation energy in IGZO TFTs under positive bias temperature stress. Solid-State Electronics, 2018, 140, 90-95.	1.4	12
58	Semiconducting Carbon Nanotube Schottky Diode and Integrated Circuit Applications. , 2018, , .		0
59	Effect of charge trap layer thickness on the charge spreading behavior within a few seconds in 3D charge trap flash memory. Semiconductor Science and Technology, 2018, 33, 10LT01.	2.0	6
60	Hybrid complementary inverter based on carbon nanotube and IGZO thin-film transistors with controlled process conditions. Journal of Alloys and Compounds, 2018, 762, 456-462.	5.5	13
61	Three-Dimensional Printed Poly(vinyl alcohol) Substrate with Controlled On-Demand Degradation for Transient Electronics. ACS Nano, 2018, 12, 6006-6012.	14.6	43
62	Degradation on the Current Saturation of Output Characteristics in Amorphous InGaZnO Thin-Film Transistors. IEEE Transactions on Electron Devices, 2018, 65, 3243-3249.	3.0	2
63	Highly transparent tactile sensor based on a percolated carbon nanotube network. AIP Advances, 2018, 8, 065109.	1.3	11
64	Synaptic Device Network Architecture with Feature Extraction for Unsupervised Image Classification. Small, 2018, 14, e1800521.	10.0	19
65	Comprehensive separate extraction of parasitic resistances in MOSFETs considering the gate bias-dependence and the asymmetric overlap length. Microelectronics Reliability, 2018, 85, 66-70.	1.7	7
66	19â€3: <i>Late-News Paper:</i> Universal Method to Determine the Dynamic NBIS―and PBSâ€induced Instabilities on Selfâ€eligned Coplanar InGaZnO Thinâ€film Transistors. Digest of Technical Papers SID International Symposium, 2018, 49, 232-235.	0.3	2
67	Pattern Recognition Using Carbon Nanotube Synaptic Transistors with an Adjustable Weight Update Protocol. ACS Nano, 2017, 11, 2814-2822.	14.6	272
68	Experimental decomposition of the positive bias temperature stress-induced instability in self-aligned coplanar InGaZnO thin-film transistors and its modeling based on the multiple stretched-exponential functions. Journal of the Society for Information Display, 2017, 25, 98-107.	2.1	25
69	Analysis and Modeling on the pH-Dependent Current Drift of Si Nanowire Ion-Sensitive Field Effect Transistor (ISFET)-Based Biosensors. Journal of Nanoscience and Nanotechnology, 2017, 17, 3146-3150.	0.9	1
70	A SONOS device with a separated charge trapping layer for improvement of charge injection. AIP Advances, 2017, 7, .	1.3	4
71	21â€4: <i>Distinguished Paper</i> : Experimental Decomposition of the Positive Bias Temperature Stressâ€induced Instability in Selfâ€eligned Coplanar InGaZnO Thinâ€film Transistors and its Modeling based on the Multiple Stretchedâ€exponential Functions. Digest of Technical Papers SID International Symposium. 2017. 48. 298-301.	0.3	8
72	Sampling Time and pH-Dependences of Silicon Nanowire Ion-Sensitive Field-Effect Transistor-Based Biosensors. Journal of Nanoscience and Nanotechnology, 2017, 17, 3257-3260.	0.9	2

#	Article	IF	CITATIONS
73	Fabrication and characterization of Pt/Al2O3/Y2O3/In0.53Ga0.47As MOSFETs with low interface trap density. Applied Physics Letters, 2017, 110, .	3.3	17
74	Systematic Decomposition of the Positive Bias Stress Instability in Self-Aligned Coplanar InGaZnO Thin-Film Transistors. IEEE Electron Device Letters, 2017, 38, 580-583.	3.9	44
75	Band-Bending Effect in the Characterization of Subgap Density-of-States in Amorphous TFTs Through Fully Electrical Techniques. IEEE Electron Device Letters, 2017, 38, 199-202.	3.9	3
76	Semiconducting carbon nanotube network thin-film transistors with enhanced inkjet-printed source and drain contact interfaces. Applied Physics Letters, 2017, 111, 173108.	3.3	14
77	Charge and dielectric effects of biomolecules on electrical characteristics of nanowire FET biosensors. Applied Physics Letters, 2017, 111, .	3.3	19
78	Transparent, Flexible Strain Sensor Based on a Solution-Processed Carbon Nanotube Network. ACS Applied Materials & Interfaces, 2017, 9, 26279-26285.	8.0	134
79	Determination of individual contact interfaces in carbon nanotube network-based transistors. Scientific Reports, 2017, 7, 5453.	3.3	7
80	Enhanced sensing of gas molecules by a 99.9% semiconducting carbon nanotube-based field-effect transistor sensor. Applied Physics Letters, 2017, 111, .	3.3	20
81	Fabrication of InGaAs-on-Insulator Substrates Using Direct Wafer-Bonding and Epitaxial Lift-Off Techniques. IEEE Transactions on Electron Devices, 2017, 64, 3601-3608.	3.0	20
82	Flammable carbon nanotube transistors on a nitrocellulose paper substrate for transient electronics. Nano Research, 2017, 10, 87-96.	10.4	37
83	Compact Two-State-Variable Second-Order Memristor Model. Small, 2016, 12, 3320-3326.	10.0	24
84	Logic circuits composed of flexible carbon nanotube thin-film transistor and ultra-thin polymer gate dielectric. Scientific Reports, 2016, 6, 26121.	3.3	29
85	Comparative study of piezoresistance effect of semiconducting carbon nanotube-Polydimethylsiloxane nanocomposite strain sensor. , 2016, , .		3
86	Ink-jet printed semiconducting carbon nanotube ambipolar transistors and inverters with chemical doping technique using polyethyleneimine. Applied Physics Letters, 2016, 109, .	3.3	11
87	Comprehensive evaluation of early retention (fast charge loss within a few seconds) characteristics in tube-type 3-D NAND flash memory. , 2016, , .		11
88	Three-Dimensional Fin-Structured Semiconducting Carbon Nanotube Network Transistor. ACS Nano, 2016, 10, 10894-10900.	14.6	16
89	Hybrid Open Drain Method and Fully Current-Based Characterization of Asymmetric Resistance Components in a Single MOSFET. IEEE Transactions on Electron Devices, 2016, 63, 4196-4200.	3.0	7
90	The <inline-formula> <tex-math notation="LaTeX">\$gamma \$ </tex-math> &lt;/inline-formula&gt;-Fe<sub>2</sub>O<sub>3</sub>Nanoparticle Assembly-Based Memristor Ratioed Logic and Its Optical Tuning. IEEE Electron Device Letters, 2016, 37, 986-989.</inline-formula>	3.9	5

#	Article	IF	CITATIONS
91	Intrinsic threshold switching responses in AsTeSi thin film. Journal of Alloys and Compounds, 2016, 667, 91-95.	5.5	24
92	Investigation of optimal hydrogen sensing performance in semiconducting carbon nanotube network transistors with palladium electrodes. Applied Physics Letters, 2015, 107, .	3.3	11
93	A Study on the Degradation of In-Ga–Zn-O Thin-Film Transistors Under Current Stress by Local Variations in Density of States and Trapped Charge Distribution. IEEE Electron Device Letters, 2015, 36, 690-692.	3.9	11
94	Extraction of Propagation Delay-Correlated Mobility and Its Verification for Amorphous InGaZnO Thin-Film Transistor-Based Inverters. IEEE Transactions on Electron Devices, 2015, 62, 1504-1510.	3.0	4
95	The Effect of Gate and Drain Fields on the Competition Between Donor-Like State Creation and Local Electron Trapping in In–Ga–Zn–O Thin Film Transistors Under Current Stress. IEEE Electron Device Letters, 2015, 36, 1336-1339.	3.9	21
96	Modeling and Separate Extraction Technique for Gate Bias-Dependent Parasitic Resistances and Overlap Length in MOSFETs. IEEE Transactions on Electron Devices, 2015, 62, 1063-1067.	3.0	5
97	TCAD-Based Simulation Method for the Electrolyte–Insulator–Semiconductor Field-Effect Transistor. IEEE Transactions on Electron Devices, 2015, 62, 1072-1075.	3.0	26
98	A Highly Responsive Silicon Nanowire/Amplifier MOSFET Hybrid Biosensor. Scientific Reports, 2015, 5, 12286.	3.3	55
99	Study on the Photoresponse of Amorphous In–Ga–Zn–O and Zinc Oxynitride Semiconductor Devices by the Extraction of Sub-Gap-State Distribution and Device Simulation. ACS Applied Materials & Interfaces, 2015, 7, 15570-15577.	8.0	82
100	Bias-Dependent Effective Channel Length for Extraction of Subgap DOS by Capacitance–Voltage Characteristics in Amorphous Semiconductor TFTs. IEEE Transactions on Electron Devices, 2015, 62, 2689-2694.	3.0	10
101	Highly uniform carbon nanotube nanomesh network transistors. Nano Research, 2015, 8, 1320-1326.	10.4	17
102	Carbon Nanotube Synaptic Transistor Network for Pattern Recognition. ACS Applied Materials & Interfaces, 2015, 7, 25479-25486.	8.0	120
103	Dual-Sweep Combinational Transconductance Technique for Separate Extraction of Parasitic Resistances in Amorphous Thin-Film Transistors. IEEE Electron Device Letters, 2015, 36, 144-146.	3.9	17
104	Numerical study of read scheme in one-selector one-resistor crossbar array. Solid-State Electronics, 2015, 114, 80-86.	1.4	28
105	Physical Origins and Analysis of Negative-Bias Stress Instability Mechanism in Polymer-Based Thin-Film Transistors. IEEE Electron Device Letters, 2014, 35, 396-398.	3.9	2
106	High-performance thin-film transistors produced from highly separated solution-processed carbon nanotubes. Applied Physics Letters, 2014, 104, .	3.3	23
107	Investigation of Sensor Performance in Accumulation- and Inversion-Mode Silicon Nanowire pH Sensors. IEEE Transactions on Electron Devices, 2014, 61, 1607-1610.	3.0	7
108	Investigation on the negative bias illumination stress-induced instability of amorphous indium-tin-zinc-oxide thin film transistors. Applied Physics Letters, 2014, 105, .	3.3	26

#	Article	IF	CITATIONS
109	Characterization and Capacitive Modeling of Target Concentration-Dependent Subthreshold Swing in Silicon Nanoribbon Biosensors. IEEE Electron Device Letters, 2014, 35, 587-589.	3.9	6
110	Short-Channel Transistors Constructed with Solution-Processed Carbon Nanotubes. ACS Nano, 2013, 7, 798-803.	14.6	83
111	Inkjet printed polymer SRAM-cell design for flexible FPGA with physical parameter-based TFT model. , 2013, , .		3
112	A novel SiNW/CMOS hybrid biosensor for high sensitivity/low noise. , 2013, , .		10
113	Investigation of Silicon Nanowire Gate-All-Around Junctionless Transistors Built on a Bulk Substrate. IEEE Transactions on Electron Devices, 2013, 60, 1355-1360.	3.0	103
114	A pH sensor with a double-gate silicon nanowire field-effect transistor. Applied Physics Letters, 2013, 102, .	3.3	46
115	Characterization of density-of-states and parasitic resistance in a-InGaZnO thin-film transistors after negative bias stress. Applied Physics Letters, 2013, 102, 143502.	3.3	15
116	Single-Scan Monochromatic Photonic Capacitance-Voltage Technique for Extraction of Subgap DOS Over the Bandgap in Amorphous Semiconductor TFTs. IEEE Electron Device Letters, 2013, 34, 1524-1526.	3.9	42
117	P.14: <i>Distinguished Poster Paper</i> : Separate Extraction Technique for Intrinsic Donor―and Acceptorâ€like Densityâ€ofâ€States over Fullâ€Energy Range Subâ€Bandgap in Amorphous Oxide Semiconductor Thin Film Transistors by Using Oneâ€Shot Monochromatic Photonic Capacitanceâ€Voltage Characteristics. Digest of Technical Papers SID International Symposium. 2013. 44, 1033-1036.	r 0.3	1
118	Latch-up based bidirectional npn selector for bipolar resistance-change memory. Applied Physics Letters, 2013, 103, .	3.3	21
119	High performance gallium-zinc oxynitride thin film transistors for next-generation display applications. , 2013, , .		24
120	Fully Transfer Characteristic-Based Technique for Surface Potential and Subgap Density of States in p-Channel Polymer-Based TFTs. IEEE Electron Device Letters, 2013, 34, 1521-1523.	3.9	5
121	Terahertz time-domain spectroscopy of anisotropic complex conductivity tensors in silicon nanowire films. Applied Physics Letters, 2012, 100, 211102.	3.3	12
122	Comparative study of solution-processed carbon nanotube network transistors. Applied Physics Letters, 2012, 101, 112104.	3.3	30
123	Addressable Nanowire Field-Effect-Transistor Biosensors With Local Backgates. IEEE Transactions on Electron Devices, 2012, 59, 2507-2511.	3.0	7
124	Physical Observation of a Thermo-Morphic Transition in a Silicon Nanowire. ACS Nano, 2012, 6, 2378-2384.	14.6	11
125	A Nonpiecewise Model for Long-Channel Junctionless Cylindrical Nanowire FETs. IEEE Electron Device Letters, 2012, 33, 155-157.	3.9	58
126	Nonvolatile memory with graphene oxide as a charge storage node in nanowire field-effect transistors. Applied Physics Letters, 2012, 100, .	3.3	11

Sung-Jin Choi

#	Article	IF	CITATIONS
127	A transistor-based biosensor for the extraction of physical properties from biomolecules. Applied Physics Letters, 2012, 101, 073703.	3.3	71
128	An Underlap Channel-Embedded Field-Effect Transistor for Biosensor Application in Watery and Dry Environment. IEEE Nanotechnology Magazine, 2012, 11, 390-394.	2.0	80
129	A New Charge-Pumping Technique for a Double-Gated SOI MOSFET Using Pulsed Drain Current Transients. IEEE Transactions on Electron Devices, 2012, 59, 241-246.	3.0	2
130	A Compact Model of Quantum Electron Density at the Subthreshold Region for Double-Gate Junctionless Transistors. IEEE Transactions on Electron Devices, 2012, 59, 1008-1012.	3.0	86
131	Silicon Nanowire All-Around Gate MOSFETs Built on a Bulk Substrate by All Plasma-Etching Routes. IEEE Electron Device Letters, 2011, 32, 452-454.	3.9	39
132	Interface-Trap Analysis by an Optically Assisted Charge-Pumping Technique in a Floating-Body Device. IEEE Electron Device Letters, 2011, 32, 84-86.	3.9	5
133	Nonvolatile Memory by All-Around-Gate Junctionless Transistor Composed of Silicon Nanowire on Bulk Substrate. IEEE Electron Device Letters, 2011, 32, 602-604.	3.9	68
134	Investigation of Size Dependence on Sensitivity for Nanowire FET Biosensors. IEEE Nanotechnology Magazine, 2011, 10, 1405-1411.	2.0	24
135	Simple Analytical Bulk Current Model for Long-Channel Double-Gate Junctionless Transistors. IEEE Electron Device Letters, 2011, 32, 704-706.	3.9	160
136	Transformable Functional Nanoscale Building Blocks with Wafer-Scale Silicon Nanowires. Nano Letters, 2011, 11, 854-859.	9.1	16
137	High performance platinum-silicided p-type Schottky barrier metal-oxide-semiconductor field-effect transistors scaled down to 30 nm. Journal of Vacuum Science and Technology B:Nanotechnology and Microelectronics, 2011, 29, .	1.2	3
138	Sensitivity of Threshold Voltage to Nanowire Width Variation in Junctionless Transistors. IEEE Electron Device Letters, 2011, 32, 125-127.	3.9	285
139	A Polydimethylsiloxane (PDMS) Sponge for the Selective Absorption of Oil from Water. ACS Applied Materials & Interfaces, 2011, 3, 4552-4556.	8.0	606
140	Vertically Integrated Unidirectional Biristor. IEEE Electron Device Letters, 2011, 32, 1483-1485.	3.9	19
141	Analysis of Transconductance \$(g_{m})\$ in Schottky-Barrier MOSFETs. IEEE Transactions on Electron Devices, 2011, 58, 427-432.	3.0	32
142	Detection of a Nanoscale Hot Spot by Hot Carriers in a Poly-Si TFT Using Polydiacetylene-Based Thermoresponsive Fluorometry. IEEE Transactions on Electron Devices, 2011, 58, 1570-1574.	3.0	2
143	An Extraction Method of the Energy Distribution of Interface Traps by an Optically Assisted Charge Pumping Technique. IEEE Transactions on Electron Devices, 2011, 58, 3667-3673.	3.0	7
144	A Full-Range Drain Current Model for Double-Gate Junctionless Transistors. IEEE Transactions on Electron Devices, 2011, 58, 4219-4225.	3.0	138

#	Article	IF	CITATIONS
145	Bioâ€Inspired Complementary Photoconductor by Porphyrinâ€Coated Silicon Nanowires. Advanced Materials, 2011, 23, 3979-3983.	21.0	29
146	An Optically Assisted Program Method for Capacitorless 1T-DRAM. IEEE Transactions on Electron Devices, 2010, 57, 1714-1718.	3.0	6
147	P-Channel Nonvolatile Flash Memory With a Dopant-Segregated Schottky-Barrier Source/Drain. IEEE Transactions on Electron Devices, 2010, 57, 1737-1742.	3.0	4
148	Dopant-Segregated Schottky Source/Drain FinFET With a NiSi FUSI Gate and Reduced Leakage Current. IEEE Transactions on Electron Devices, 2010, 57, 2902-2906.	3.0	8
149	Analytical Modeling of a Nanogap-Embedded FET for Application as a Biosensor. IEEE Transactions on Electron Devices, 2010, 57, 3477-3484.	3.0	115
150	Optically Assisted Charge Pumping on Floating-Body FETs. IEEE Electron Device Letters, 2010, 31, 1365-1367.	3.9	4
151	Double-Gate Nanowire Field Effect Transistor for a Biosensor. Nano Letters, 2010, 10, 2934-2938.	9.1	162
152	An underlap field-effect transistor for electrical detection of influenza. Applied Physics Letters, 2010, 96, .	3.3	57
153	Analysis and Evaluation of a BJT-Based 1T-DRAM. IEEE Electron Device Letters, 2010, 31, 393-395.	3.9	15
154	High-Performance Polycrystalline Silicon TFT on the Structure of a Dopant-Segregated Schottky-Barrier Source/Drain. IEEE Electron Device Letters, 2010, 31, 228-230.	3.9	14
155	Fin Width \$(W_{m fin})\$ Dependence of Programming Characteristics on a Dopant-Segregated Schottky-Barrier (DSSB) FinFET SONOS Device for a NOR-Type Flash Memory Device. IEEE Electron Device Letters, 2010, 31, 71-73.	3.9	6
156	Fin-Width Dependence of BJT-Based 1T-DRAM Implemented on FinFET. IEEE Electron Device Letters, 2010, 31, 909-911.	3.9	15
157	Investigation of the source-side injection characteristic of a dopant-segregated Schottky barrier metal-oxide-semiconductor field-effect-transistor. Applied Physics Letters, 2009, 95, 063508.	3.3	4
158	Gate-to-Source/Drain Nonoverlap Device for Soft-Program Immune Unified RAM (URAM). IEEE Electron Device Letters, 2009, 30, 544-546.	3.9	12
159	Fully Depleted Polysilicon TFTs for Capacitorless 1T-DRAM. IEEE Electron Device Letters, 2009, 30, 742-744.	3.9	14
160	Characterization of current injection mechanism in Schottky-barrier metal-oxide-semiconductor field-effect transistors. Applied Physics Letters, 2009, 95, .	3.3	0
161	Refinement of Unified Random Access Memory. IEEE Transactions on Electron Devices, 2009, 56, 601-608.	3.0	5
162	Resistive-Memory Embedded Unified RAM (R-URAM). IEEE Transactions on Electron Devices, 2009, 56, 2670-2674.	3.0	4

#	Article	IF	CITATIONS
163	Improvement of the Sensing Window on a Capacitorless 1T-DRAM of a FinFET-Based Unified RAM. IEEE Transactions on Electron Devices, 2009, 56, 3228-3231.	3.0	3
164	Enhancement of Program Speed in Dopant-Segregated Schottky-Barrier (DSSB) FinFET SONOS for <emphasis emphasistype="smcaps">NAND</emphasis> -Type Flash Memory. IEEE Electron Device Letters, 2009, 30, 78-81.	3.9	21
165	High Injection Efficiency and Low-Voltage Programming in a Dopant-Segregated Schottky Barrier (DSSB) FinFET SONOS for nor-type Flash Memory. IEEE Electron Device Letters, 2009, 30, 265-268.	3.9	11
166	Gate-Induced Drain-Leakage (GIDL) Programming Method for Soft-Programming-Free Operation in Unified RAM (URAM). IEEE Electron Device Letters, 2009, 30, 189-191.	3.9	20
167	Energy-Band-Engineered Unified-RAM (URAM) Cell on Buried \$hbox{Si}_{1 - y}hbox{C}_{y}\$ Substrate for Multifunctioning Flash Memory and 1T-DRAM. IEEE Transactions on Electron Devices, 2009, 56, 641-647.	3.0	2
168	A Bulk FinFET Unified-RAM (URAM) Cell for Multifunctioning NVM and Capacitorless 1T-DRAM. IEEE Electron Device Letters, 2008, 29, 632-634.	3.9	23